Acta Astronautica 158 (2019) 444–459

Contents lists available at ScienceDirect

Acta Astronautica

journal homepage: www.elsevier.com/locate/actaastro

Including analytically reduced chemistry (ARC) in CFD applications

Anne Felden[a,*], Perrine Pepiot[b], Lucas Esclapez[a], Eleonore Riber[a], Bénédicte Cuenot[a]

[a] CERFACS, CFD Team, 42 Av. Gaspard Coriolis, 31057, Toulouse, France
[b] Sibley School of Mechanical and Aerospace Engineering, Cornell University, Itaca, NY, 14853, USA

ARTICLE INFO

Keywords:
Reduced chemistry
Large eddy simulation
Gas turbines

ABSTRACT

Reacting numerical simulations today are often based on either fitted global reaction schemes, comprised of a few empirical reactions, or pre-tabulated laminar flame solutions computed with detailed chemistry. Although both methods can accurately predict global quantities such as laminar flame speed and burnt gas composition, they have significant limitations. In particular, neither are able to directly and adequately describe the complexity of pollutant chemistry. In the context of reducing harmful emissions of the next generation of aeronautical combustors, however, including these needed additional kinetic details in combustion simulations is becoming essential. Direct integration of detailed chemistry in accurate turbulent combustion models is not a viable option in the foreseeable future, because of excessive computational demands and numerical stiffness. In this context, Analytically Reduced Chemistry (ARC) represents an attractive compromise between accuracy and efficiency, and is already employed in relatively complex Direct Numerical Simulations (DNS) and Large Eddy Simulations (LES). ARCs are knowledge-based compact mechanisms retaining only the most relevant kinetic information as extracted directly, and without fitting, from detailed chemical models using specialized reduction techniques (important species identification through graph search, lumping of species with similar features, short-living species identification, etc.). In recent years, several multi-step efficient and automated reduction tools have been developed, enabling the easy generation of ARCs with minimum input and knowledge from the user. The main objective of this paper is to present a review of ARCs for fuels ranging from methane to aviation kerosene surrogates, recently derived with such a multi-step automated reduction tool: YARC. Information about the applicability and range of validity of each derived mechanism are given, along with further references. Each one was specifically derived to be convenient to use in CFD; in particular, the stiffness was regarded as a key factor and the final number of transported species never exceeds thirty. In a final section, the great potential of the methodology is illustrated in a multi-phase, reactive LES application where the fuel is a real multi-component transportation fuel. To that end, an ARC based on a Jet A described by the novel Hybrid Chemistry (HyChem) approach is coupled with the Dynamically Thickened Flame LES (DTFLES) model and directly integrated into the LES solver AVBP. A Lagrangian spray description is used. Results are compared to experimental data in terms of temperature and major species (CO_2, H_2O, CO, NO) mass fractions, leading to very satisfying results.

1. Introduction

In the context of increasing air traffic and energy demand in the aeronautic sector, experienced over the past 30 years, the pollutants released by the combustion of aviation fuels (kerosenes, biofuels) have become a major worldwide concern. This awareness has motivated considerable actions from engine manufacturers towards the development of a new fuel-efficient generation of aeroengine combustors with low emissions. However, the simultaneous improvement of efficiency and minimization of harmful emissions results in somewhat contradictory design trends, further complicated by constraining safety and operability specifications [1]. In particular, the intricacies of the combustion process -still not nearly enough understood today, prevent a direct control of all the parameters, prompting further research. The advent of numerical simulation tools such as Reynolds averaged Navier-Stokes (RANS), Direct Numerical Simulation (DNS), and Large Eddy Simulation (LES) [2–5], coupled to the continuously increasing available computational power, now provides a way to tackle these issues with more and more accuracy [6]. Numerical simulations of complex devices that include the description of turbulent reacting flows, are progressively becoming affordable at a design stage [6,7]. However, the capability to predict pollutant emissions relies heavily upon the fidelity

* Corresponding author.
E-mail address: amfelden@lbl.gov (A. Felden).

https://doi.org/10.1016/j.actaastro.2019.03.035

Available online 13 March 2019

Nomenclature

ARC	Analytically reduced chemistry
CSP	Computational singular perturbation
CVR/CPR	Constant volume/pressure reactor
DNS	Direct numerical simulation
DRG	Directed relation graph
DRGASA	DRG aided sensitivity analysis
DRGEP	DRG error propagation
DRGX	DRG with expert knowledge
DTFLES	Dynamic thickened flame LES model
HyChem	Hybrid chemistry
IRZ	Inner recirculation zone
LDI	Lean direct injection
LES	Large Eddy Simulation
LOI	Level of importance
NSCBC	Navier-Stokes characteristic boundary conditions
PCA	Principal component analysis
PSR	Perfectly stirred reactor
QSS	Quasi-steady state
RANS	Reynolds-Averaged Navier-Stokes
SDF	Strained diffusion flame
UPF	Unstrained premixed flame
YARC	Yet another reduction code

of the chemistry description [8], and insights must be provided on both the dynamics of the fluid and the chemistry of the flame, as well as on their possible interactions. Unfortunately, the accurate computation of combustion chemistry -including interactions with turbulence in the context of LES, remains challenging in numerical simulations [4,9,10]. One main reason is that combustion proceeds through complex and highly non-linear processes that involve up to hundreds of different chemical compounds, with various associated time and length scales. As a result, if the progress made during the second half of the 20th century regarding fundamental measurements and quantum chemistry calculations led to an improved understanding of the underlying physics, allowing the development of accurate and comprehensive detailed kinetic mechanisms, taking them into account without any simplification in large scale computations prohibitively increases the computational time and often induces stiffness in the resolved equations.

The most common simplification employed to include detailed kinetic mechanisms in CFD today is to assume that thermo-chemical evolutions in the composition/temperature space can be parameterized by a reduced set of variables. Usually, these include the mixture fraction and the progress variable. With this assumption, any thermochemical quantity of interest can be retrieved by interpolation in a database, precomputed with detailed chemistry [11–17]. This approach drastically reduces the number of transport equations to be solved, and is thus very computationally efficient. On the downside, simulations using tabulation are very much dependent upon the type of canonical configurations chosen to build the look-up table [18,19] (premixed or diffusion archetypes, in modern tabulation techniques). If recent studies have addressed this issue [20–22], it remains often necessary to resort to a few additional controlling parameters, which can eventually lead to excessive memory requirements and Input/Output cost. Another major disadvantage, particularly in LES of complex real geometries, is that interactions between the flame and the flow are oversimplified. Taking into account complex phenomena such as preferential diffusion, dilution, liquid fuel, heat losses or slow pollutant chemistry then requires additional modeling efforts that can be far from trivial: additional parametrization variables are introduced, for which transport equations must be solved [23–25], resulting in additional unclosed terms. In that regard, there is also a need to formulate *a priori* assumptions about the nature of the flow.

Another classical approach consists in using globally-fitted chemical mechanisms [26–31]. The idea is to split the global reaction of fuel oxidation into empirical intermediate steps. Usually, from one to four steps are considered, involving important intermediates such as CO or H_2. The reaction rate constants are expressed in an Arrhenius form, the various parameters of which are fitted against detailed chemistry results or experiments within a specified operating range, to yield good results on global flame parameters (namely, temperature and laminar flame speed). Here also, the method is CPU-efficient due to the small number of transported variables. However, the physics of the problem (i.e., the true chemical pathways) is completely lost, and only a very narrow range of operating conditions is covered. Furthermore, pollutant information is either unavailable (soot, NOx) or inaccurate (CO). A possible remedy to these drawbacks is to employ so-called “hybrid” techniques, relying upon the definition of a progress variable compatible with that of a tabulation technique so as to retrieve missing information (soot precursors, intermediate species, NO_x) from a look-up table [32,33]. However, the drawbacks associated with tabulation are retrieved.

Driven by the same necessity to reduce the high dimensionality of detailed chemistry for further investigation, physics-oriented reduction techniques have been developed [34–37]. By performing a targeted mathematical analysis of the timescales and species fluxes in a detailed reaction mechanism, the main competing chemical pathways involved in specific combustion applications can be identified, and unnecessary kinetic information can be safely discarded. The fundamental aspect of reduced mechanisms obtained by these methods, referred to below as Analytically Reduced Chemistry or ARC, is that expressions for the evolution of all species of interest are analytically obtained, and rely directly upon the detailed chemistry model. In particular, the reaction rate constants are not modified. Of particular interest with such a chemistry description is the fact that when integrated directly in a CFD code, flame/flow interactions are not frozen, and there is no need to formulate *a priori* assumptions about the nature of the flow or the complexity of the configuration. Additionally, if the key kinetic pathways are properly identified and retained, one can reasonably expect a reduced chemical model to yield realistic species compositions even outside of its strictly demonstrated domain of validity, adding well-needed robustness to complex reactive simulations.

Two different types of reduction can be applied to a detailed reaction mechanism, to yield either a *skeletal* mechanism, where a set of unnecessary species and reactions has been discarded, or an *analytical* mechanism, where reactions are combined in order to express the

Table 1
Common methods to obtain ARC. Note that the provided list of references is non-exhaustive.

Skeletal reduction	Sensitivity Analysis [39,40], Principal Component Analysis [35,41] Path Flux analysis [42,43], Jacobian Investigations [36] Graph search: DRG [44], DRGX [45], DRGASA [46], DRGEP [47] Chemical Lumping [48,49]
Analytical reduction	Quasi-Steady State approximation: via CSP pointers [50,51], via LOI [52,53], via production/consumption analysis [54], via error estimation [36], via chemical intuition [34]

evolution of a few well-chosen species through algebraic relations. Both reductions have their respective set of tools and techniques, an overview of which is provided in Table 1. The most common procedure for skeletal reduction is to first identify and eliminate *redundant* species (and associated reactions), before identifying and eliminating *redundant* reactions (terminology from Ref. [38]). Techniques pertaining to analytical reduction mostly deal with stiffness removal through an investigation of the system's timescales. Usually, it is the combination of both reductions, skeletal followed by analytical, that leads to a fully reduced mechanism, or an ARC.

The concept is not new: ARCs have been obtained in a brute force way, through sensitivity and uncertainty analysis using experience, chemical intuition, and a trial-and-error approach even long before the advent of modern computers [34,35]. In fact, the Quasi-Steady State (QSS) approximation, used in the analytical part of the reduction, dates back to the early 1920's, where it was referred to as the Bodenstein method [55]. In particular, detailed mechanisms for the oxidation of hydrogen and methane have been widely investigated [34,56] during the second half of the last century; noteworthy are the series of papers by Turanyi and co-workers on the subject [57]. The limitation in these early studies to small hydrocarbons is due to several facts [6]. First, the investigated mechanisms were all that computational capacities were able to handle at that time. Moreover, it has long been known that the heaviest hydrocarbon mechanisms rely strongly on lighter hydrocarbon mechanisms, from which they derive their main features. More importantly, a comprehensive understanding of the underlying kinetic processes of heavier hydrocarbons is a rather recent development and still an active area of research. Finally, when considering real fuels, a complication arise from their multicomponent nature and uncertainties concerning their composition.

In the past decade, however, the growing need for more detailed kinetic information in relatively large and complex numerical simulations has motivated efforts towards the development of accurate ARCs for large hydrocarbons and real fuels, specifically tailored for an implementation in CFD codes [58–60]. This interest outside of the “pure chemistry” community has driven the emergence of efficient numerical tools to help perform kinetic reductions in a systematic fashion. These tools usually implement several techniques amongst the ones listed in Table 1, in so-called *multi-step* reduction strategies, in order to reach the maximum level of reduction possible. Typically, retaining from 10 to 30 species (depending upon the fuel) is nowadays affordable in relatively large LES [61–69]. In this framework, the challenge of real fuel emulation is usually tackled through the definition of a surrogate [70] composed of only a handful of compounds. However, this method introduces competing and interfering chemical pathways which can significantly complexify the reduction process. An alternative approach for real, multicomponent jet fuels was recently proposed [71], termed HyChem. It assumes that fuel pyrolysis is fast and decoupled from the oxidation of decomposed products. It has been shown that deriving ARCs of HyChem models comprised of about 30 species, that are still able to reproduce well the combustion chemistry behaviors of real fuels, is feasible [69,72].

In the present context, where ARCs are on the verge of becoming affordable at a design stage, the authors believe that it is of interest to compile recently derived LES-compliant ARCs for various hydrocarbons, in order to make them available to the community. As a first step towards achieving this goal, the present paper summarizes ARCs derived over the past 5 years with the multi-step reduction tool YARC [53]. Information about the applicability and range of validity of each derived mechanism are given, along with further references. Note that when deriving an ARC, the ultimate reference is the original detailed kinetic mechanism, and therefore, exhaustive comparisons between experiments and YARC-derived ARCs fall outside of the scope of this paper. All ARCs derived in this study are based upon well-accepted detailed kinetic mechanisms, and readers are referred to the original publications for their validation.

The paper is organized as follows: Section 2 briefly introduces the multi-step reduction concept, focusing specifically on the tool YARC [53]. Then, Section 3 summarizes YARC-derived ARCs for various hydrocarbons ranging from methane to aviation kerosene. These reduced mechanisms together with a few other LES-compliant ARCs reported in the literature are analyzed, and the data are employed to address CFD-specific issues such as the usual size and stiffness to be expected from such a chemistry description. Finally, Section 4 presents a detailed example of ARC use in a two-phase flow, kerosene fueled LES application to demonstrate the capabilities offered by this type of chemistry description.

2. The YARC tool

2.1. Principle of multi-step reduction strategies

The different reduction techniques can be classified according to the level of reduction they allow to achieve, as done in Table 1. It is obvious that techniques belonging to different categories complement each other, and that one cannot hope to obtain the best possible ARC by employing only one of them. In fact, the “know-how” developed in the combustion community over the past decades reveals that to perform an efficient reduction, it is best to proceed in steps, starting with a skeletal reduction before searching for potential QSS species. This led to the design of multi-step reduction strategies, where each step is enabled by borrowing from techniques belonging to each category. Note that the skeletal reduction can be comprised of several steps. To illustrate the discussion, Table 2 reports three multi-step reduction strategies reported in the literature: consistently with the previous remarks, all follow the same organization.

The required inputs to such multi-step reductions consist of a detailed mechanism, a set of *targets*, and some error tolerance. Targets, in this context, stand for both the canonical problem employed for the reduction, and the quantities for the ARC to reproduce with the best accuracy. For example, if say, the ultimate goal is to investigate a sooting ethylene non-premixed jet, generating an ARC for ethylene oxidation with a good prediction of soot precursors (like acetylene for example) based on 1-D counterflow configurations is desirable.

Note that as many reduction techniques are well designed for numerical implementation, these multi-step reduction strategies are usually automated, in multi-step reduction tools. Pioneering programs were exclusively post-processors, requiring outputs from pre-existing chemistry simulation codes, and often producing results that required further adjustment to be used in chemistry or CFD solvers. This was the case of KINAL(C) [78] or CARM [79], post-processing CHEMKIN simulations [80], or the S-STEP [81] working on results from RUN-1DL [82]. More recent tools are fully coupled with chemistry solvers, and are thus able to sequentially run the canonical test cases, carry the

Table 2
Literature review of multi-step reduction strategies. See Table 1 for references to the reduction techniques.

	Strategy I [73]	Strategy II: YARC [53]	Strategy III: KINALC [38]
STEP I Species reduction	DRG(X/ASA)	DRGEP Chemical Lumping	Jacobian investigations
STEP II Reactions reduction	DRG(X/ASA)	DRGEP	PCA
STEP III	QSS via CSP pointers	QSS via LOI	QSS via error estimation
Examples	[73,74] and more online [76]:	[33,47,49,60] and more online [77]:	[75] and more online [57]:

model reduction based upon the results, perform the subsequent numerical integration of the derived set of differential equations -thus simplifying the crucial validation step, and properly format the result for further use in CFD codes. This is the case, for example, of YARC [53], employed in this work, or the tool developed recently at CORIA [83]. Obviously, designing a reduction process as systematic as possible is highly desirable in order to facilitate the derivation of reduced mechanisms for non-experienced users.

2.2. YARC

The multi-step automated reduction tool YARC (in its first version) was developed a few years ago by one of the authors [53]. The tool consists of a series of libraries written in Pearl, implementing the DRGEP and Chemical Lumping for skeletal reduction, and the LOI for QSS selection, as summarized in Table 2 (references given in Table 1). It is fully coupled with the chemistry solver FlameMaster [84], which solves the targeted canonical cases to reproduce. The reduction can be performed on a combination of various cases, by targeting a number of important quantities such as, for example, specific species mass fractions. The canonical cases and targets employed to guide the reduction will be discussed in more depth in subsection 2.3.

During the reduction process, YARC generates several reduced mechanisms with increasing error level, as well as many output files containing information about each reduced mechanism. In particular, error levels pertaining to each targeted quantity can be easily monitored. The overall reduction process with YARC is illustrated on Fig. 1. Eventually, given a set of user-specified error levels on each targeted quantity, the best possible reduced mechanism is readily identified.

2.3. Targeted canonical test cases and targeted quantities

The canonical test cases employed to perform and assess the validity of the reduction of a detailed mechanism include 0-D and 1-D configurations. Belonging to the first category are constant volume or pressure batch reactors (CVR/CPR) and perfectly stirred reactors (PSR), while belonging to the second category are steady unstretched premixed laminar flames (UPF), as well as steady strained laminar diffusion flames (SDF).

When employing batch reactors, the quantity of interest is the auto-ignition timing (τ_{ig}). When using PSR, the quantity of interest is the minimum residence time, commonly accepted as a marker of extinction. In the present work, both quantities are estimated based upon the gradient of temperature. In laminar premixed or diffusion flame configurations, it is obviously of interest to recover the correct evolution of the temperature and major species (fuel, OH, CO, NO, etc.) across flame fronts. But global quantities such as the laminar flame speed (s_l), the burnt gas temperature (T_b), the global fuel consumption ($\dot{\omega}_F^{tot}$), or the global production of major pollutants such as CO or NO ($\dot{\omega}_{CO/NO}^{tot}$) across flame fronts are also often monitored. In the present work, s_l is taken to be the inlet velocity (in UPF); while the global consumption/formation of a specific species X is estimated as:

$$\dot{\omega}_X^{tot} = \int_{c<0.98} \dot{\omega}_X \, dx \tag{1}$$

where x is the spatial coordinate and c is the progress variable, based on the mass fraction of CO and CO_2 [10].

In the following (Section 3), for clarity of exposition and to ensure that a broad range of ARCs are covered, the validity of the derived ARCs is only demonstrated on a selected subset of canonical test cases, namely CVR and UPF; and for a limited range of operability consistent with respective derivation ranges. However, the range of validity (known to us) is specified for each ARC, along with references to further validation and/or applications for the interested reader.

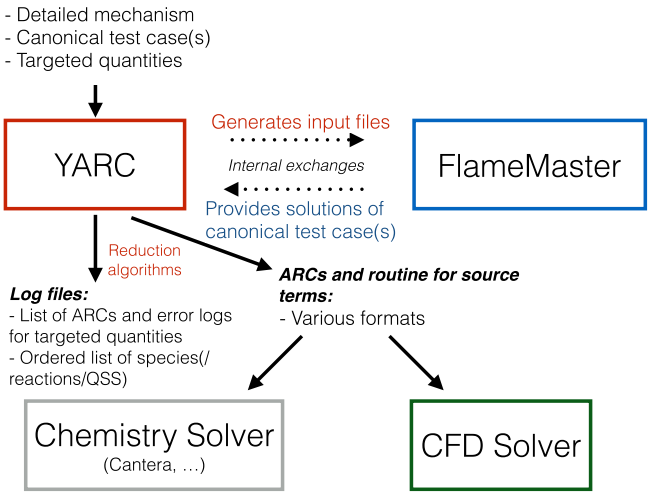

Fig. 1. Diagram of YARC

3. From methane to kerosene: a collection of ARC

All mechanisms that are presented in this section are available in a Cantera format online [77]. Alternatively, the transported and QSS species are listed for each reduced mechanism, along with references to the detailed mechanism, so that it is possible to reconstruct each ARC easily. To that end, the species names are those of the original detailed mechanisms, and the reader is referred to the reference publications for further details regarding specific species properties. As mentioned in the introduction, the performances of an ARC are evaluated with respect to the detailed mechanism from which it is derived, and not directly to experimental data. Indeed, when deriving an ARC, the ultimate reference is the original detailed kinetic mechanism, and therefore, exhaustive comparisons between experiments and YARC-derived ARCs fall outside of the scope of this paper.

3.1. Methane

Two ARCs for methane-air combustion have been derived, based on either the GRIMech 2.11 [85] (ARC_GRI211) or the GRIMech 3.0 [86] (ARC_GRI30) detailed mechanisms. They were both designed to target premixed applications, and to preserve NO accuracy (global and local production); using the same canonical test cases and set of targets. Details about the derivation and validation range as well as the list of retained transported and QSS species are provided in Table 3. Both ARCs are shown to have validation range that extends outside of their respective derivation range. To illustrate this, Fig. 2 (a) reports laminar flame speed values for several initial equivalence ratios and pressures. In fact, the ARC_GRI211 has also been validated on HT auto-ignition (AI) test cases, for a broad range of initial pressures (see Fig. 2 (b)).

Aside from these global quantities, the local flame structure is also very well predicted by each ARC (Fig. 3 (a) & (b)).

3.2. Ethylene

An ARC for ethylene-air oxidation has been derived, based on the Narayanaswamy detailed mechanism [88] (referred to as N&B hereafter) which is part of a modular comprehensive reaction mechanism still under development.[1] It was designed to target premixed applications with sooting tendencies and to preserve CO accuracy (global and local production). C_2H_2 is recognized as a major soot precursor and is targeted by the reduction. Details about the derivation and validation

[1] http://krithikasivaram.github.io/.

Table 3
YARC derived ARCs for methane combustion.

Fuel/Oxidant	Methane/Air	Methane/Air
Purpose	Premixed applications and NO analysis	Premixed applications and NO analysis
Detailed mechanism	GRI 2.11 [85]	GRI 3.0 [86]
Number of transported species/reactions/QSS	22/320/18	22/266/21
Transported species	H H_2 O O_2 OH H_2O HO_2 H_2O_2 CH_3 CH_4 C_2H_2 C_2H_4 C_2H_6 CO CO_2 CH_2O CH_3OH NO NO_2 N_2 N_2O HCN	same set
QSS species	C CH CH_2 1-CH_2 C_2H_3 C_2H_5 HCO CH_3O HCCO N NH NH_2 NNH HNO NCO HCNO HNCO HOCN	same set + CH_2OH H_2CN CN
Targeted canonical test cases	UPF: P = 1 atm T = 300 K ϕ = [0.6–1.4]	UPF: P = 1 atm T = 300 K ϕ = [0.6–1.4]
Targeted quantities	UPF: s_l, T_b, CO, NO	UPF: s_l, T_b, CO, NO
Validation range (for the targeted quantities)	UPF: P = [1–6] bars T = [300−700] K ϕ = [0.4–1.6] AI: P = [1–15] bars T = [1000–3000] K ϕ = [0.5–1.5]	UPF: P = [1–6] bars T = [300−700] K ϕ = [0.4–1.6]
Refs (more validations)	[33,65,66,87]	[33]

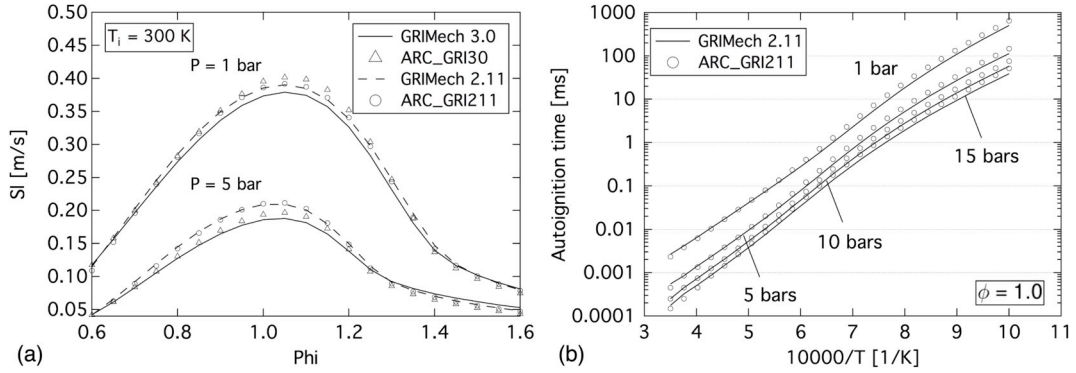

Fig. 2. (a) Example of performances of the ARC_GRI211 and ARC_GRI30 on methane-air UPF test cases. (b) Example of performances of the ARC_GRI211 on canonical CVR test cases. Comparisons are performed with the relevant detailed mechanism.

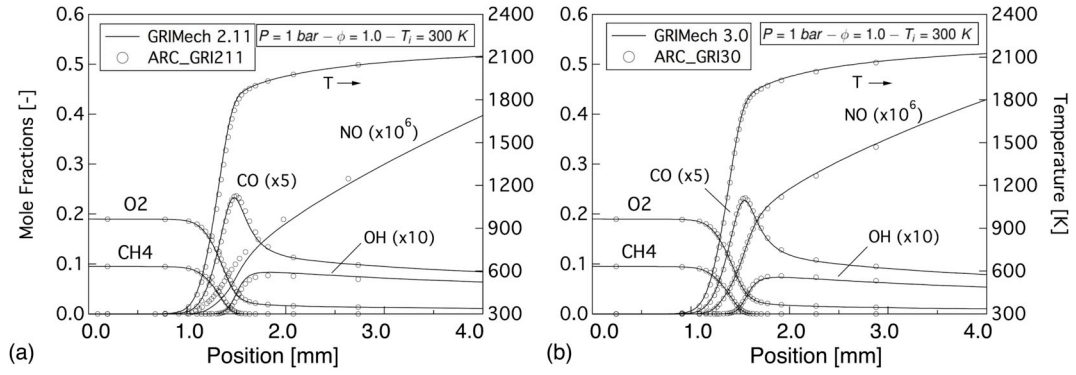

Fig. 3. Evolution of selected major species and temperature across a canonical UPF for P = 1 bar, T_i = 300 K and ϕ = 1.0 with (a) the ARC_GRI211 and (b) the ARC_GRI30. Comparisons are performed with the relevant detailed mechanism.

range as well as the list of retained transported and QSS species are provided in Table 4. Fig. 4 illustrates the performances of this ARC mechanism (ARC_NB) on various canonical test cases (targeted and non-targeted by the derivation).

3.3. Propane

An ARC for propane-air combustion has been derived, based on the Jerzembeck (High Temperature) version of the LLNL mechanism for *iso*-octane and *n*-heptane mixtures [89,90]. It was designed to target premixed applications (with emphasis on lean premixed applications), and to preserve CO accuracy (global and local production). Details

Table 4
YARC derived ARC for ethylene combustion.

Fuel/Oxidant	Ethylene/Air
Purpose	Premixed applications, CO and soot analysis
Detailed mechanism	N&B [88]
Number of transported species/reactions/QSS	18/355/11
Transported species	H H_2 O O_2 OH H_2O HO_2 H_2O_2 CH_3 CH_4 C_2H_2 C_2H_4 C_2H_6 CO CO_2 CH_2O CH_2CO N_2
QSS species	C CH S−CH_2 T-CH_2 C_2H_3 C_2H_5 HCO HCCO CH_2CHO CH_3CHO C_2H_5O
Targeted canonical test cases	UPF: P = 3 atm T = 300 K ϕ = [0.5–1.5] AI: P = 3 atm T = [1300–1700] K ϕ = [0.5–1.5]
Targeted quantities	UPF: s_l, T_b, CO, CO_2, OH, C_2H_2 AI: τ_{ig}, T_{eq}, CO, CO_2, OH, C_2H_2
Validation range (for the targeted quantities)	UPF: P = [1–10] bars T = [300 − 700] K ϕ = [0.5–2.5] AI: P = [1–40] bars T = [1200–3000] K ϕ = [0.5–1.5]
Refs (more validations)	[60,67]

Table 5
YARC derived ARC for propane combustion.

Fuel/Oxidant	Propane/Air
Purpose	Premixed applications and CO analysis
Detailed mechanism	LLNL [89,90]
Number of transported species/reactions/QSS	22/173/12
Transported species	H H_2 O O_2 OH H_2O HO_2 H_2O_2 CH_3 CH_4 C_2H_2 C_2H_4 C_2H_6 C_3H_6 C_3H_8 CO CO_2 CH_2O CH_3O_2 CH_3O_2H C_3H_5O N_2
QSS species	CH_2(S) C_2H_3 C_2H_5 C_3H_5-a i-C_3H_7 n-C_3H_7 i-$C_3H_7O_2$ n-$C_3H_7O_2$ HCO CH_3O HCCO CH_2CHO
Targeted canonical test cases	UPF: P = 1 atm T = 288 K ϕ = [0.6–1.6]
Targeted quantities	UPF: s_l, T_b, CO, CO_2
Validation range (for the targeted quantities)	UPF: P = [1–5] bars T = [288 − 300] K ϕ = [0.6–1.6] AI: P = [1–20] bars T = [1500–3000] K ϕ = 1.0
Refs (more validations)	[91]

about the derivation and validation range as well as the list of retained transported and QSS species are provided in Table 5. Fig. 5 illustrates the performances of this ARC mechanism (ARC_LLNL) on various canonical test cases (targeted and non-targeted by the derivation). Note that if the mechanism is able to correctly account for τ_{ig} over a large operating range it should not be employed for high temperature auto-ignition, due to large errors on the final temperature (about 6% for T > 1600 K).

3.4. Heptane

An ARC for heptane-air combustion has been derived, based on the Jerzembeck (High Temperature) version of the LLNL mechanism for *iso*-octane and *n*-heptane mixtures [89,90]. It was designed to target premixed applications, and to preserve CO/CO_2 equilibrium. Details

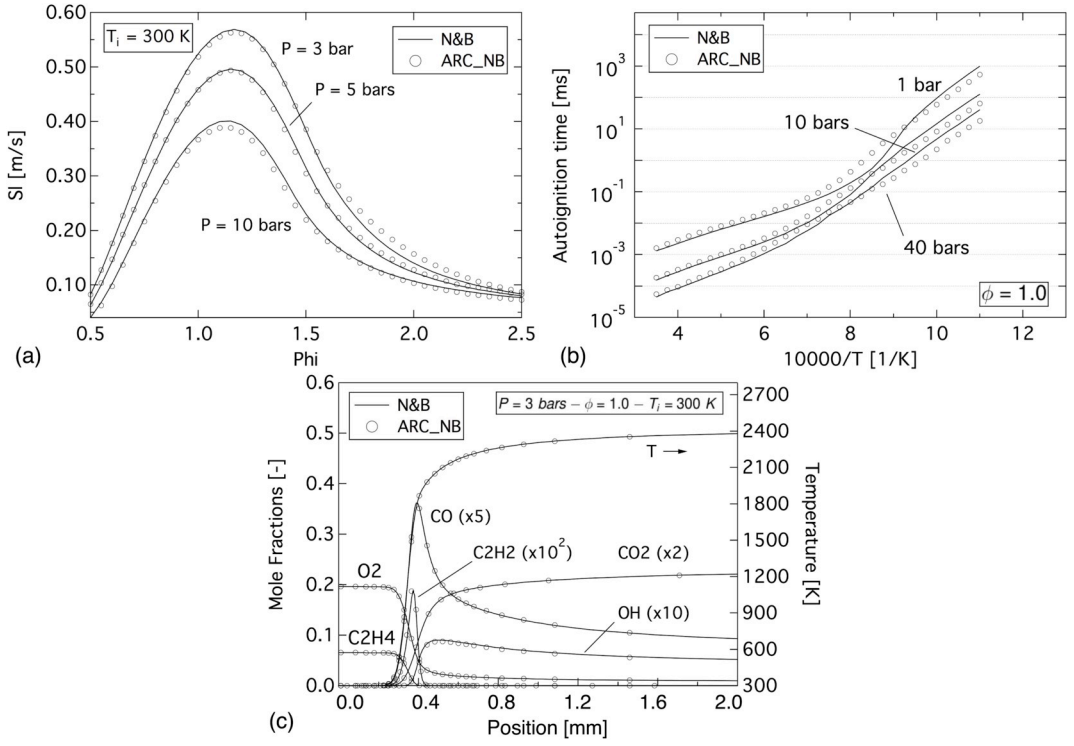

Fig. 4. Example of performances of the ARC_NB on (a) canonical UPF test cases and (b) canonical CVR test cases. (c) Evolution of selected major species and temperature across a canonical UPF for P = 3 bar, T_i = 300 K and ϕ = 1.0, computed with the ARC_NB. All comparisons are performed with the N&B detailed mechanism.

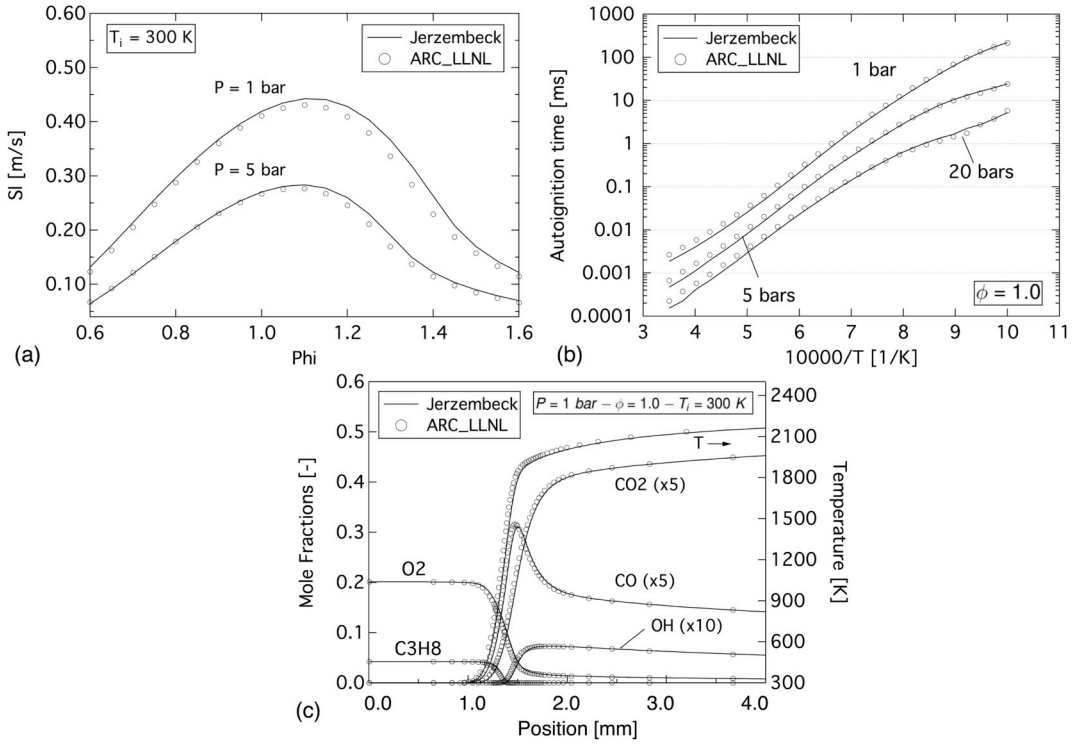

Fig. 5. Example of performances of the ARC_LLNL on (a) canonical UPF test cases and (b) canonical CVR test cases. (c) Evolution of selected major species and temperature across a canonical UPF for P = 1 bar, T_i = 300 K and ϕ = 1.0, with the ARC_LLNL. Comparisons are performed with the relevant detailed mechanism [89].

about the derivation and validation range as well as the list of retained transported and QSS species are provided in Table 6. Fig. 6 illustrates the performances of this ARC mechanism (ARC_LLNL_C7H16) on targeted canonical test cases.

3.5. *n*-dodecane

Two ARCs for *n*-dodecane-air combustion have been derived based on the JetSurF 1.0-l [92], a simplified version of JetSurF 1.0 [93]. The JetSurF 1.0-l features a lumped model for *n*-alkane cracking, and the detailed USC Mech II [94] for the pyrolysis and oxidation of C1−C4 hydrocarbons. Both were designed to target premixed applications at high pressure and temperature, representative of realistic operating conditions in high overall pressure ratio engines [95]. The ARC_JetSurf_NOx was specifically derived to preserve NO accuracy (global and local production), while the ARC_JetSurf was derived to preserve accuracy of the major soot precursor, namely, acetylene (C_2H_2), and to extend to smaller operating temperatures. Details about the derivation and validation range as well as the list of retained transported and QSS species in each ARC are provided in Table 7. Fig. 7 illustrates the performances of the ARCs in various canonical test cases, targeted and non-targeted by the derivation. The ARC_JetSurf_NOx is able to correctly account for auto-ignition over a large operating range. The validity range of the ARC_JetSurf on UPF test cases extends to atmospheric conditions.

3.6. Jet A

3.6.1. HyChem model for the jet A POSF10325

Very often, the surrogate formulation for a real fuel like aviation kerosene relies upon the selection of a few representative hydrocarbon components. Typically, from one to four components are retained, including *n/iso/cyclo*-alkanes and aromatics [96]. However, an alternative approach was recently proposed, based on experimental observations: the HyChem model [97,98]. The methods relies on the assumption that any fuel, no matter how complex it is, would first decomposes into a handful of small molecules, and that it is the distribution of these pyrolysis products that would impacts the subsequent radical buildup and heat release rate. The pyrolysis product pool is dominated by hydrogen (H_2), methane (CH_4), ethylene (C_2H_4), propene (C_3H_6), *iso*-butene (i-C_4H_8), 1-butene (1-C_4H_8), benzene (C_6H_6) and toluene (C_7H_8). It follows that, the combustion process can be decomposed into a fuel pyrolysis step and a subsequent oxidation process of the pyrolysis product. Detailed kinetic models for particular real fuels can thus be

Table 6
YARC derived ARCs for heptane combustion.

Fuel/Oxidant	Heptane/Air
Purpose	Premixed applications
Detailed mechanism	LLNL [89,90]
Number of transported species/ reactions/QSS	25/210/27
Transported species	H H_2 O O_2 OH H_2O HO_2 H_2O_2 CH_3 CH_4 C_2H_2 C_2H_4 C_2H_6 C_3H_4-a C_3H_6 C_4H_6 C_4H_8-1 n-C_7H_{16} CO CO_2 CH_2O HOCHO CH_3OH CH_2CO N_2
QSS species	CH CH_2(S) CH_2 C_2H_3 C_2H_5 C_3H_2 C_3H_3 C_3H_5-a n-C_3H_7 C_4H_7 p-C_4H_9 C_5H_9 C_5H_{10}-1 C_5H_{11}-1 C_6H_{12}-1 C_7H_{15}-2 HCO CH_3O CH_3O_2 CH_3O_2H HCCO CH_2CHO CH_3CO C_2H_5O $C_2H_5O_2$ n-$C_3H_7O_2$ p-$C_4H_9O_2$
Targeted canonical test cases	UPF: P = 1 atm T = 298 K ϕ = [0.6–1.6]
Targeted quantities	UPF: s_b T_b
Validation range (for the targeted quantities)	UPF: P = [1–5] bars T = 300 K ϕ = [0.5–2.0]

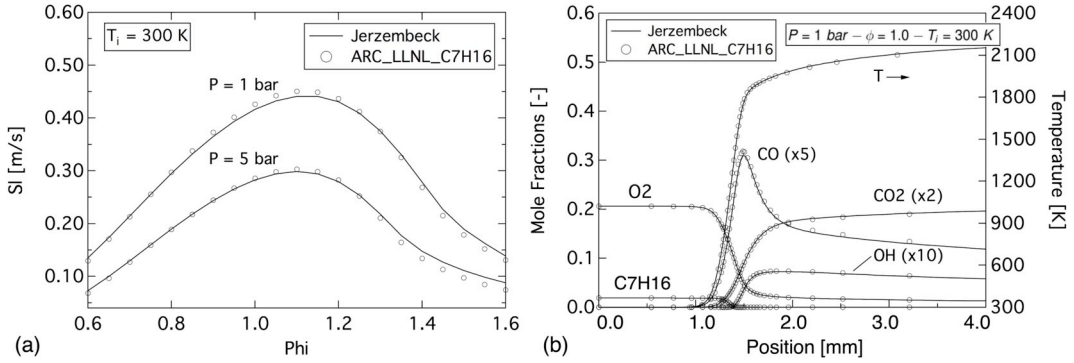

Fig. 6. Example of performances of the ARC_LLNL_C7H16 on canonical UPF test cases: (a) laminar flame speed and (b) evolution of selected major species and temperature across a canonical UPF for P = 1 bar, T_i = 300 K and ϕ = 1.0. Comparisons are performed with the relevant detailed mechanism [89,90].

obtained by merging a pyrolysis mechanism comprised of a few lumped reactions, yielding the composition of the primary pyrolysis products, and a detailed foundational kinetic mechanism. The "fuel", in that case, is a mono-component lumped species. Its pyrolysis kinetic rates and products are determined from shock tube and flow reactor pyrolysis and oxidative pyrolysis studies. It has been demonstrated that HyChem models capture shock-tube ignition delay times, laminar flame speeds and non-premixed flame extinction rates [98] over a wide range of pressure, temperature and equivalence ratio for at least a dozen jet, rocket and gasoline fuels. Examples for the jet and rocket fuels are given in Xu et al. [98].

The specific HyChem model considered for the reduction is that of an average, commercial Jet A fuel (POSF10325), which was procured from the Shell Mobile refinery in June 2013 as a part of tests conducted by the National Jet Fuel Combustion Program. Its properties are summarized in Table 8.

3.6.2. Derivation of ARCs for the jet A POSF10325

Based on the HyChem model, two ARCs for the oxidation of Jet A have been derived. They were both designed to target partially premixed applications under atmospheric conditions, and to properly account for the decomposition of the main pyrolysis products (C_2H_4, C_6H_6, C_2H_2). One of the ARCs, referred to as the ARC_HYCHEM_NOx, was supplemented with a reduced version of the Luche NO_x sub-mechanism [99] to account for NO global and local production. Details about the derivation and validation range as well as the list of retained transported and QSS species are provided in Table 9. Figs. 8 and 9 illustrate the performances of both ARCs on various canonical test cases, targeted and non-targeted by the derivation. In particular, note that the reduced mechanisms are still valid (provided that the detailed mechanism is still valid !) under relatively high operating pressures, more representative of current aero-engines design.

3.7. ARC for LES of turbulent combustion: general trends

3.7.1. Size of ARCs

Fig. 10 reports correlations between species and reactions contained in a collection of ARCs. Two ARCs for methane-air combustion and one ARC for ethylene-air oxidation reported in the literature [76] were added to those presented in this paper. Data from an in-house ARC for

Table 7
YARC derived ARCs for *n*-dodecane combustion.

Fuel/Oxidant	*n*-dodecane/Air	*n*-dodecane/Air
Purpose	Partially premixed applications NO and CO analysis	Partially premixed applications CO and soot analysis
Detailed mechanism	JetSurF 1.0 [92,93]	JetSurF 1.0 [92,93]
Number of transported species/reactions/QSS	27/452/20	25/373/27
Transported species	H H_2 O O_2 OH H_2O HO_2 CH_3 CH_4 C_2H_2 C_2H_4 C_2H_6 C_3H_6 C_4H_6 C_5H_{10} C_6H_{12} n-$C_{12}H_{26}$ $C_4H_8$1 CO CO_2 CH_2O CH_2CO NO NO_2 N_2 N_2O HCN	H H_2 O O_2 OH H_2O HO_2 H_2O_2 CH_3 CH_4 C_2H_2 C_2H_4 C_2H_6 C_3H_6 C_4H_6 C_4H_8 − 1 C_5H_{10} C_6H_6 C_6H_{12} n-$C_{12}H_{26}$ CO CO_2 CH_2O CH_2CO N_2
QSS species	H_2O_2 CH CH_2 CH_2* C_2H C_2H_3 C_2H_5 aC_3H_5 nC_3H_7 C_4H_7 HCO CH_3O HCCO CH_2CHO N NH NH_2 HNO NCO HNCO	CH CH_2 CH_2* C_2H H_2CC C_2H_3 C_2H_5 C_3H_3 pC_3H_4 aC_3H_5 CH_3CHCH nC_3H_7 C_4H_2 C_4H_4 iC_4H_5 C_4H_5-2 C_4H_7 o-C_6H_4 C_6H_5 $C_6H_5CH_3$ C_2O HCO CH_3O HCCO CH_2CHO H_2C_4O C_6H_5CO
Targeted canonical test cases	UPF: P = 10 bars T = 700 K ϕ = [0.6–1.4]	UPF: P = 9 bars T = [400 − 700] K ϕ = [0.6–1.4]
Targeted quantities	UPF: s_l, T_b, CO, NO	UPF: s_l, T_b, CO, C_2H_2
Validation range (for the targeted quantities)	UPF: P = [5–15] bars T = [700 − 900] K ϕ = [0.5–2.0] AI: P = [10–40] bars T = [1100–2900] K ϕ = [0.5–1.5]	UPF: P = [1–10] bars T = [300 − 700] K ϕ = [0.5–2.0]
Refs (more validations)	[33]	

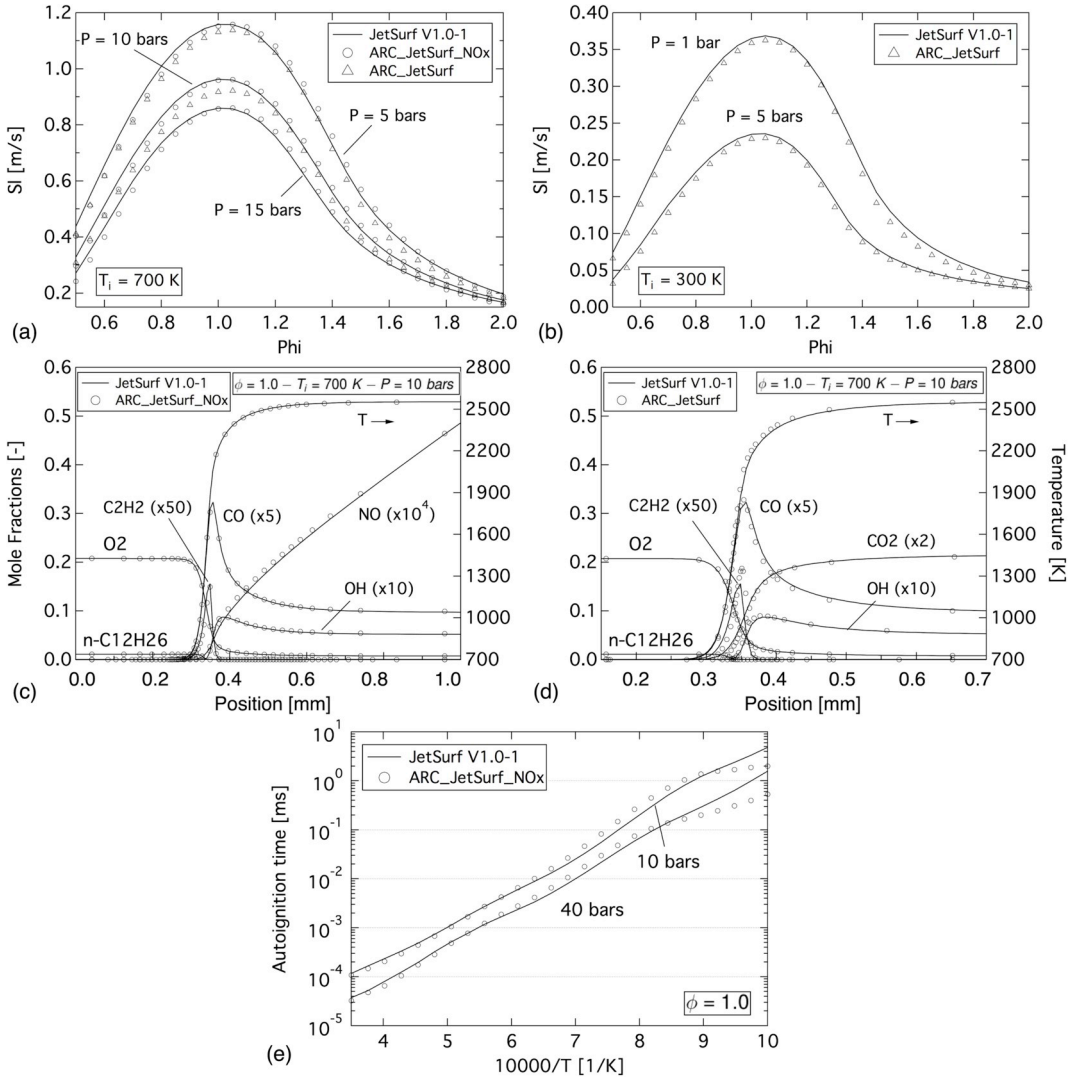

Fig. 7. Example of performances of the ARC_JetSurf and ARC_JetSurf_NOx on canonical UPF test cases: (a)–(b) laminar flame speed versus equivalence ratio for different pressure and initial temperature, (c)–(d) evolution of selected major species and temperature across a canonical UPF for P = 10 bars, T_i = 700 K and ϕ = 1.0. (d) Example of CVR cases results with the ARC_JetSurf_NOx. Comparisons are performed with the relevant detailed mechanism [92,93].

iso-octane combustion were also added, to bridge the gap between the small hydrocarbons and kerosene surrogates. Each circle represents one ARC. Red circles represent ARCs containing a NO_x sub-mechanism, blue circles represent ARCs with the prospect of soot modeling, and dark circles represent ARCs not targeting pollutants.

One interesting observation is that the number of reactions to consider (Fig. 10 (d)) seem to be greatly impacted by the decision to include the formation of pollutants. It is particularly true of NO, requiring to take into account many additional pathways involving azoted species. Of course, these additional reactions are associated with an additional set of species, that must also be accounted for in the ARC. However, as can be seen in Fig. 10 (a)&(b), the overcost of species is less pronounced than the overcost of reactions. This causes the correlation between species and reactions contained in ARCs retaining a NO_x sub-mechanism to stray from the theoretical line of [9], reported in Fig. 10 (d). This is an important observation, indicating that, at least in terms of number of species to transport, any hydrocarbon can be accommodated in CFD.

3.7.2. Species to consider

Another interesting observation from the analysis of each ARC, either reported in the literature or YARC-derived, is that there appears to be a "core" of 14 species systematically identified as necessary and thus, retained whatever the hydrocarbon. These are: H, H_2, O, O_2, OH, H_2O,

Table 8
Properties of the Jet-A POSF10325.

Molecular formula	Composition (mass fraction [%])					Mol. Weight
	Aromatics	*iso*-Paraffins	*n*-Paraffins	Cycloparaffins	Alkenes	[g/mol]
$C_{11.4}H_{22.1}$	18.66	29.45	20.03	31.86	< 0.001	158.6
H/C	Δh_c [MJ/kg]	DCN	T_{10} [K]	$T_{90} - T_{10}$ [K]	μ_l(300 K) [mPa s]	ρ_l(300 K) [kg/m^3]
1.91	43.1	48.3	450.0	67.8	1.37	794

Table 9
YARC derived ARCs for Jet A combustion.

Fuel/Oxidant	Jet A (POSF10325)/Air	Jet A (POSF10325)/Air
Purpose	Partially premixed applications CO analysis	Partially premixed applications NO and CO analysis
Detailed mechanism	USC II [94] + pyrolysis steps [71,100]	USC II [94] + pyrolysis steps [71,100]
Number of transported species/reactions/QSS	27/268/12	29/518/17
Transported species	H H_2 O O_2 OH H_2O HO_2 H_2O_2 CH_3 CH_4 C_2H_2 C_2H_4 C_2H_6 C_3H_6 aC_3H_4 i-C_4H_8 C_5H_6 C_6H_6 $C_6H_5CH_3$ CO CO_2 CH_2O CH_2CO C_6H_5O $C_6H_4O_2$ N_2 POSF10325	H H_2 O O_2 OH H_2O HO_2 H_2O_2 CH_3 CH_4 C_2H_2 C_2H_4 C_2H_6 C_3H_6 i-C_4H_8 C_5H_6 C_6H_6 $C_6H_5CH_3$ CO CO_2 CH_2O CH_2CO C_6H_5O $C_6H_4O_2$ N_2 NO NO_2 HCN POSF10325
QSS species	CH_2 CH_2* C_2H_3 C_2H_5 aC_3H_5 C_6H_5 $C_6H_5CH_2$ HCO CH_3O HCCO CH_2CHO C_6H_5CHO	CH CH_2 CH_2* C_2H_3 C_2H_5 aC_3H_5 C_6H_5 HCO CH_3O HCCO CH_2CHO N NH CN H_2CN HNO NCO
Targeted canonical test cases	UPF: P = 1 bar T = 300 K ϕ = [0.8–1.3] AI: P = 1 bar T = [1300–1700] K ϕ = [0.8–1.3]	UPF: P = 1 bar T = 300 K ϕ = [0.8–1.3] AI: P = 1 bar T = [1300–1700] K ϕ = [0.8–1.3]
Targeted quantities	UPF: s_l, T_b, OH, CO, pyrolysis products AI: τ_{ig}, T, OH, CO	UPF: s_l, T_b, OH, CO, NO, pyrolysis products AI: τ_{ig}, T, OH, CO
Validation range (for the targeted quantities)	UPF: P = [1–10] bars T = [300] K ϕ = [0.5–1.5] AI: P = [1–40] bars T = [1000–3000] K ϕ = [0.5–1.5]	UPF: P = [1–10] bars T = [300] K ϕ = [0.5–1.5] AI: P = [1–40] bars T = [1000–3000] K ϕ = [0.5–1.5]
Refs (more validations)	[60,101]	[60,69]

HO_2, H_2O_2, CH_3, CH_4, CO, CO_2, CH_2O and N_2. For hydrocarbons with a carbon content of 2 or more, this list is appended with C_2H_2, C_2H_4 and C_2H_6. Note that HO_2, H_2O_2 or CH_3 are sometimes identified as potential QSS species, due to their small associated timescales. Moreover, most of the time, the 6 following species are retained as QSS: CH_2, CH_2*, C_2H_3, C_2H_5, HCO and HCCO.

If NO is of interest, NO_2, N_2O and HCN are usually retained, to account for the various NO pathways. These species are added to the list of transported species. Additionally in this case, CH becomes necessary, being a key intermediate in many thermal pathways. It is usually put in QSS.

3.7.3. Stiffness of ARCs

One major drawback associated with the use of ARC in CFD is that the chemical timescales involved can span a large range. Radical species are consumed as soon as they are produced, while the formation of NO or soot spreads over a few seconds. ARCs are thus always associated with stiffness. However, in most cases and with a careful derivation, stiffness can be reduced to a minimum by limiting the transport of species with very short associated timescales.

To that end, it is of interest to identify these “absolutely necessary” species, that are seen to induce stiffness. From an investigation of the ARCs considered in this paper, it appears that:

- For a fuel carbon content below 3, H_2O_2 is usually the species with the smallest associated timescale.
- For a fuel carbon content above 8 (typical kerosene surrogates), the fuel is usually the species with the smallest associated timescale.
- For propane and *n*-heptane, just as for many fuel species of intermediate size, the consideration of very short-lived radicals (C-4/C-5) will generally be required, complexifying the reduction process and possibly resulting in relatively stiff mechanisms.

These considerations are illustrated in Fig. 11, showing the minimum chemical timescales involved in a laminar flame under atmospheric conditions, in a collection of ARCs. The timescale evaluation is based upon a Jacobian evaluation performed with perturbations.

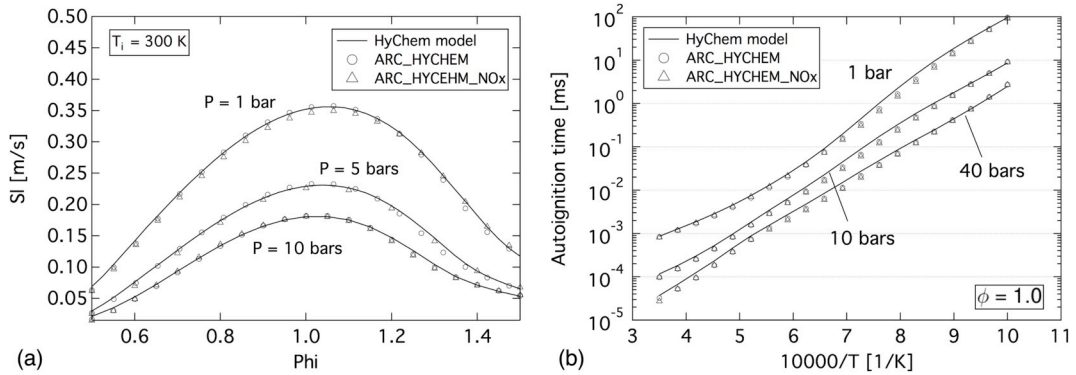

Fig. 8. Example of performances of the ARC_HYCHEM and ARC_HYCHEM_NOx on (a) canonical UPF test cases and (b) canonical CVR test cases. Comparisons are performed with the relevant detailed HyChem model [94,100].

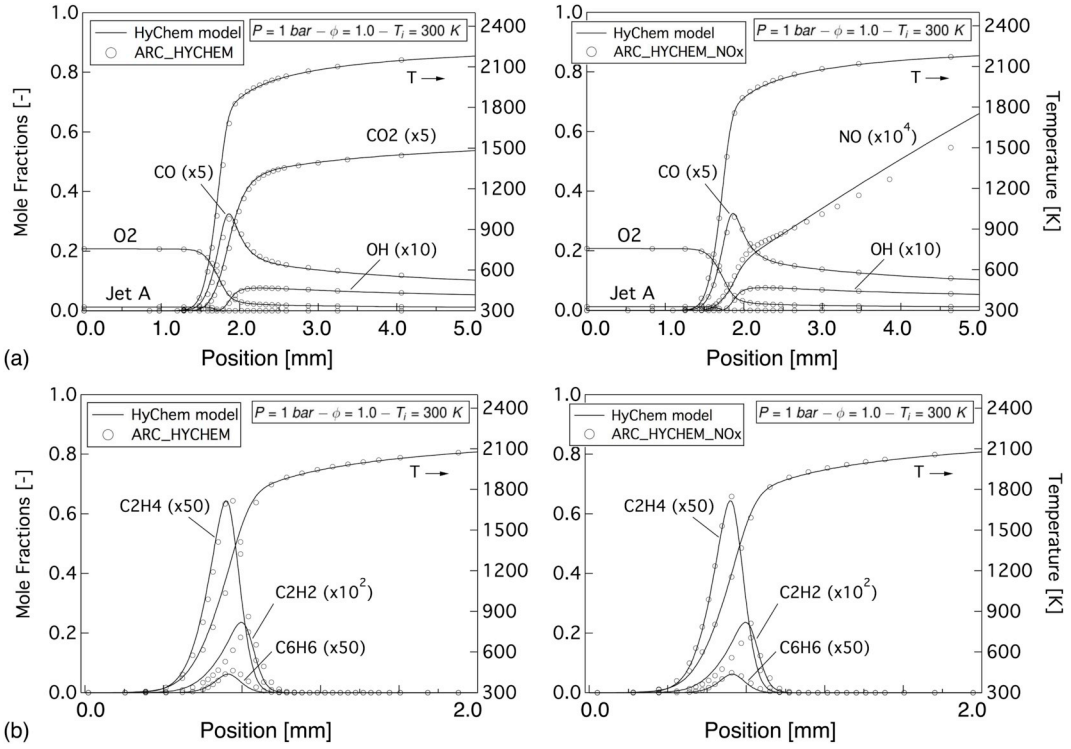

Fig. 9. Evolution of (a) selected major species and temperature and (b) major intermediates across canonical UPF for P = 1 bar, T_i = 300 K and ϕ = 1.0, with both ARCs derived based on the HyChem model. Comparisons are performed with the relevant detailed HyChem model [94,100].

4. Application to a real fuel academic burner

To demonstrate the successful implementation of ARC in a CFD solver, the Jet A reduced mechanism presented in Section 3.6 is employed to simulate an academic kerosene fueled swirled burner [69].

4.1. Configuration

Results obtained in the lean direct injection (LDI) combustor operated at NASA Glenn [102–104], and already presented in Felden et al. [69] are summarized here. The experimental facility is illustrated in

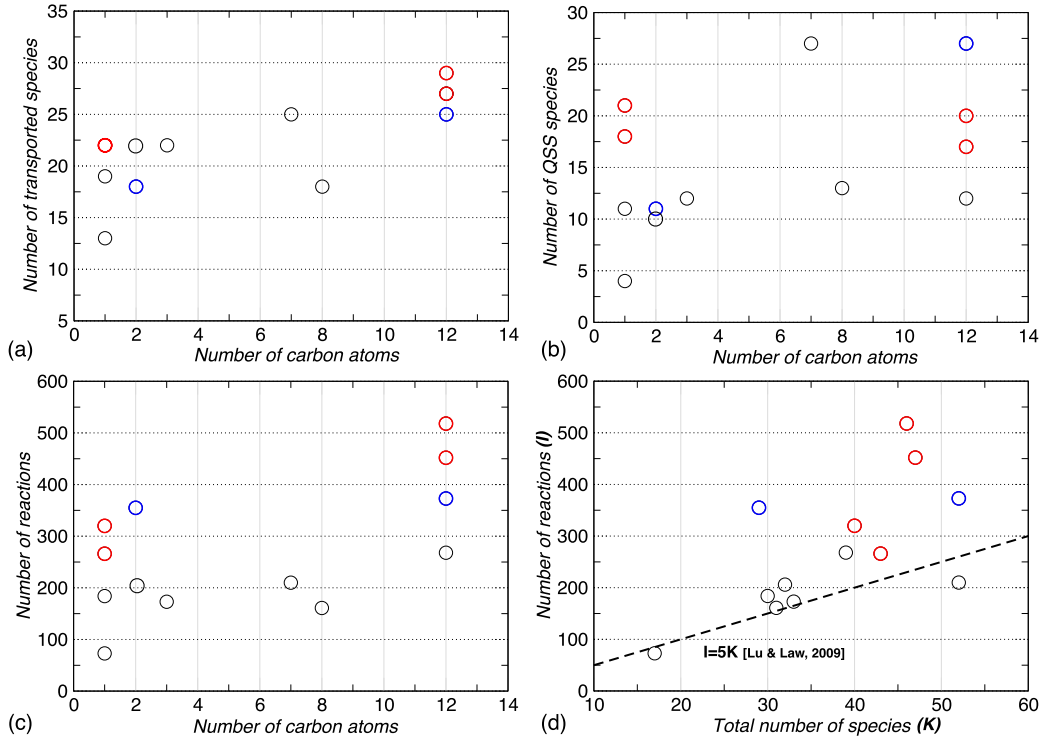

Fig. 10. Number of (a) transported species (b) QSS species (c) reactions versus number of carbon content in each hydrocarbon. (d) Number of reactions versus the total number of species contained (transported + QSS) in each ARC. The line reports the tendency observed by Lu & Law [9].

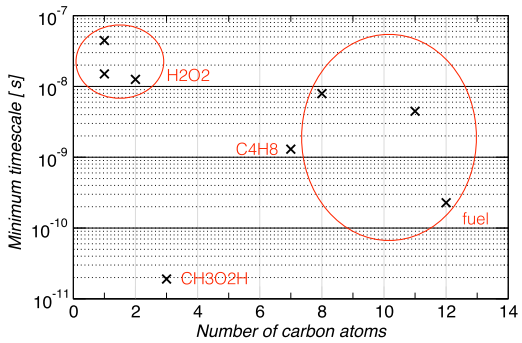

Fig. 11. Estimation of the minimum timescales involved in a canonical UPF case, under atmospheric conditions. The ARCs reported are YARC-derived ARCs, valid under atmospheric conditions.

Fig. 12(a), with details of the injection system in Fig. 12(c). Air is injected through an axial swirler composed of six helicoidal vanes inclined at 60° while fuel goes through a central PARKER pressure-swirl atomizer. The combustion chamber is a 50.8 mm × 50.8 mm x 305 mm box and has quartz windows on all sides.

The test rig is operated at ambient conditions (P = 1 atm, T = 300 K). The air and fuel mass flow rates are 8.16 g/s and 0.415 g/s respectively, which corresponds to a lean overall equivalence ratio of 0.75. Measurements of gas velocity and temperature, spray velocity and droplet size distribution are available [102,104].

4.2. Numerical setup

The LES set-up is briefly summarized in the following. Further details can be found in Felden et al. [69].

Simulations are performed with the fully compressible Navier-Stokes explicit solver AVBP solving for the conservation equations of the filtered momentum, total energy and species mass fractions, with an explicit third-order in time and space two-step Taylor-Galerkin finite element scheme for the integration of the convective fluxes [105] and a second-order Galerkin scheme for the diffusive fluxes. The LES subgrid-scale model is the SIGMA eddy-dissipation model [106] associated with constant turbulent Prandtl and Schmidt numbers, respectively ($Pr_t = Sc_t = 0.6$). The turbulent combustion model is the dynamic thickened flame (DTFLES) model [107], where the flame front is thickened so as to be sufficiently discretized by the grid, while keeping the correct consumption speed. Subgrid-scale flame wrinkling is modeled via an efficiency function, following the formulation of Charlette et al. [108]. The dilute spray is described with a Lagrangian point source approach. Evaporation is calculated with the Abramzon-Sirignano model [109] while the Schiller and Naumann correlation is used for the drag coefficient, together with Ranz-Marshall correlations for the Sherwood and Nusselt numbers.

The simulation domain, shown in Fig. 12(b) and (c), includes the injection system and the combustion chamber. The mesh is built with tetrahedra, from 0.25 mm size close to the injection system to about 3 mm size downstream, leading to over 4 millions nodes and 23 millions tetrahedra.

4.3. Results

4.3.1. Instantaneous flame structure

The instantaneous flame structure is depicted in Fig. 13 showing contours of temperature, heat release rate, velocity and several species mass fraction in a central z-normal cut plane. The flame structure is rather complex, with a main flame zone directly fed by droplets located in front of the injector ((1) in Fig. 13(a)), and secondary reaction zones located downstream close to the combustion chamber walls ((2) in Fig. 13(a)).

Iso-contours of mixture fraction in Fig. 13 displays a rich and hot torus located in the bottom part of the IRZ. The stoichiometric iso-contours identify the main reaction zone, stabilized by the fast evaporation of the smallest droplets. This massive evaporation induces strong mixture fraction gradients, resulting in diffusion flame structures with intermittent premixed flame pockets. The top half of Fig. 13(b) shows the instantaneous field of Y_{HyChem} constructed from the sum of the Jet-A, pyrolysis products and acetylene mass fractions. Y_{HyChem} is high in the rich torus, where a large amount of CO is also observed. This testifies of the variety of diffusion flame structures that can be seen in this region.

The non-null mass fraction of H_2O, CO_2 and HO_2 upstream of the secondary reaction zones (Fig. 13(e)-(f)), in the corner of the combustor, indicates that local extinction allows dilution of the incoming air with burnt gases and pyrolysis products. As this mixture is convected along the combustion chamber walls, the increasing temperature enables the formation of a lean premixed flame front.

Finally, larger droplets are found to cross both flame fronts and to burn in an isolated droplet regime throughout the combustion chamber ((3) in Fig. 13(a)). However, the present modeling approach is not able to accurately predict the combustion regime around the droplets as it essentially occurs on a subgrid scale.

4.3.2. Temperature and species statistics

The focus is given here on the validation of the temperature and species mass fraction predictions. Validations of the non-reacting and reacting velocity fields as well as spray characteristics are presented in Felden et al. [69].

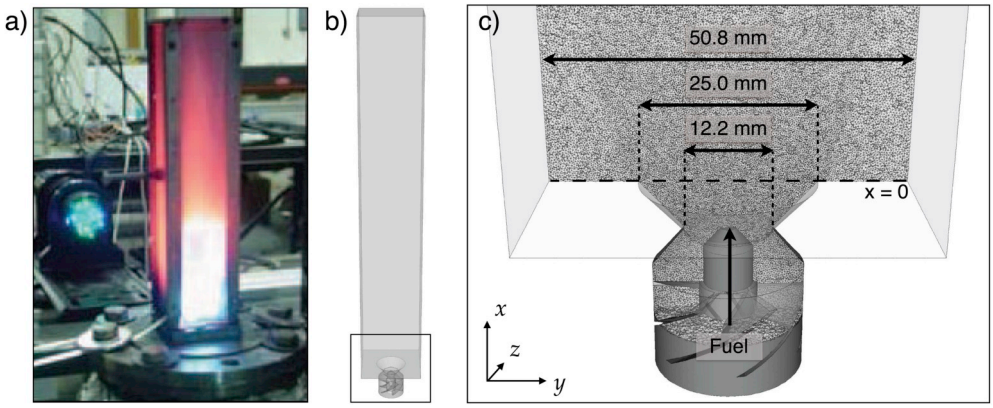

Fig. 12. a) Picture of the experimental test rig [102], b) Entire computational domain and c) Mesh resolution at the vicinity of the injection system along with system size. Adapted from Ref. [69].

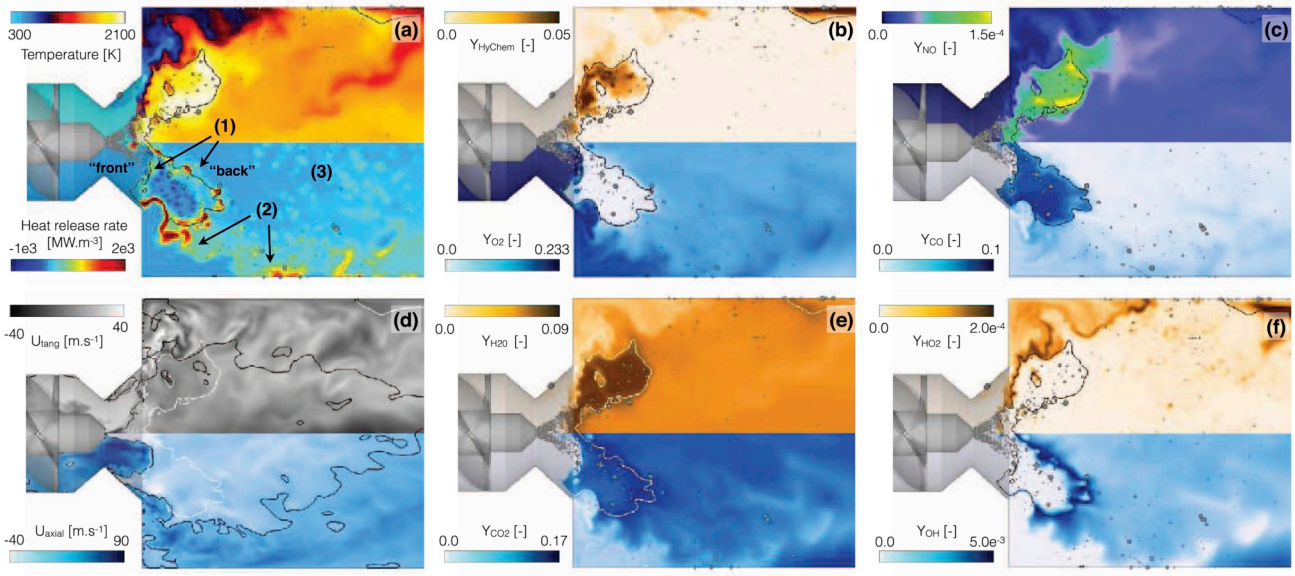

Fig. 13. Instantaneous fields in a central z-normal cut plane. (a) Temperature (top) and heat release rate (bottom), (b) summed mass fractions of fuel and pyrolysis products (top) and O_2 mass fraction (bottom), (c) NO (top) and CO (bottom) mass fractions, (e) H_2O (top) and CO_2 (bottom) mass fractions and (f) HO_2 (top) and OH (bottom) mass fractions. The black iso-line indicates stoichiometry. (d) Tangential (top) and axial (bottom) components of velocity, black iso-contours delimit the IRZ while white iso-contours indicates stoichiometry.

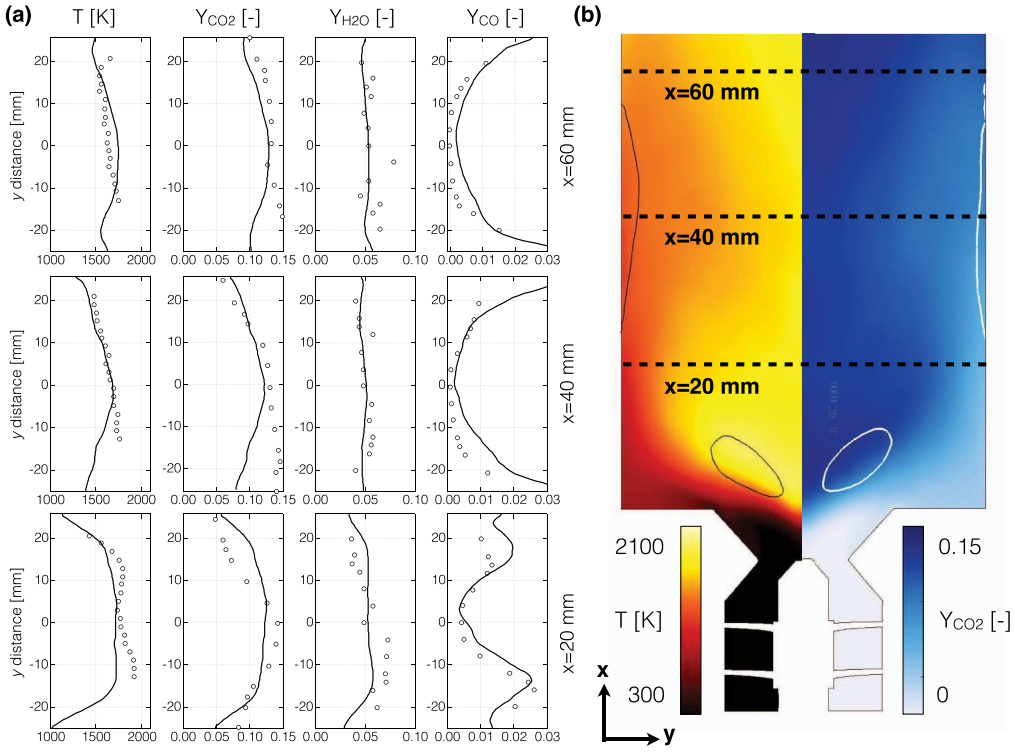

Fig. 14. (a) Profiles of time-averaged temperature and selected species (CO_2, H_2O and CO) at x = 20 mm, 40 mm and 60 mm in reacting conditions. Symbols: experiments, black line: LES. (b) Time-averaged fields of temperature and CO_2 species in a z-normal central cut plane. The iso-contour indicates the position of the stoichiometry. Adapted from Ref. [69].

Fig. 14(a) provides a comparison between experimental and LES radial profiles of temperature and major species, at three axial locations identified by horizontal dashed lines on Fig. 14(b), spanning the vicinity of the dump plane. H_2O and CO_2 evolutions are very well captured by the LES, even though the model predictions exhibit less asymmetry than in the experiments. Note that if some asymmetry is to be expected from the 6-vanes swirler, the LES results also suggest non-negligeable experimental uncertainties. A less well agreement is obtained on the temperature profiles. At x = 20 mm, the experimental profile displays a bimodal shape that is observed closer to the injection system in the LES. The same bimodal shape is seen on the LES profiles at x = 10 mm (not shown), suggesting that the main flame front is in fact shifted further upstream than in the experiments. An inspection of the mean stoichiometric iso-contours, superimposed with the mean fields of

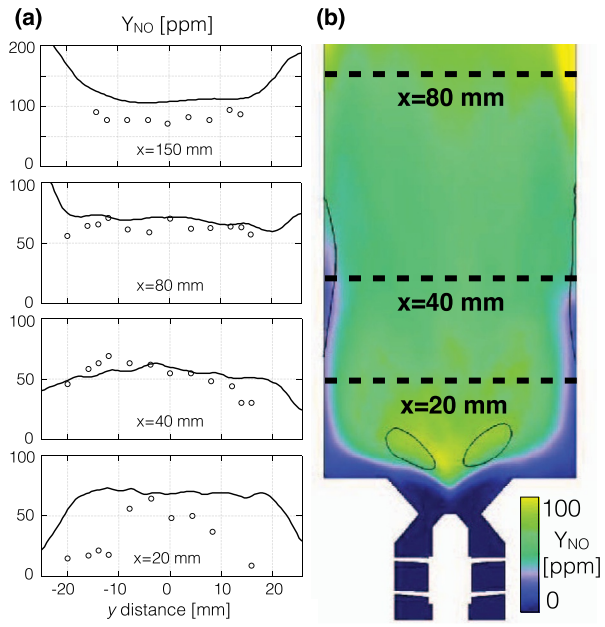

Fig. 15. (a) Profiles of time-averaged NO species at x = 20 mm, 40 mm, 80 mm and 150 mm in reacting conditions. Symbols: experiments, black line: LES. (b) Time-averaged fields of NO species in a z-normal central cut plane. The iso-contour indicates the position of the stoichiometry. Adapted from Ref. [69].

temperature and major species mass fractions in Fig. 14(b), confirms that the region of highest reactivity is preferably located upstream from the first profile location. Despite this apparent shift, however, the two peaks on the CO profile at 20 mm, representative of the early post-flame region, are well predicted by the LES. It is noted that the main flame appears lifted in both LES and experiments, which could be due to the high turbulent velocity magnitude observed close to the injector.

Downstream of the main diffusion flame region, there seems to be an accumulation of CO species along the walls, accompanied by a decrease of temperature, in both LES and experiments. It is reminded that no heat losses are included in the simulation. These phenomena are therefore attributed to the accumulation of droplets following the jet impact, leading to the formation of regions of very rich mixture fraction. Stoichiometric iso-contours along the walls, centered at x = 40 mm as seen on Fig. 14(b), confirm this analysis. For x > 60 mm, the LES temperature is seen to be overpredicted along the centerline. A closer examination of the experimental data indicates that the temperature at the outlet of the combustion chamber rig is under the theoretical adiabatic value at the overall equivalence ratio (approximately 300 K below). This difference suggests the presence of heat losses (radiation, walls, etc.) and/or incomplete combustion.

LES NO predictions are presented on Fig. 15(a) and (b). LES results are compared to experiments at four axial positions, with the last one (x = 150 mm) corresponding to the half of the combustion chamber length. NO levels are found to be higher in the core of the IRZ, in the vicinity of the first stoichiometric iso-contours where the main flame sits, and to be significantly smaller along the walls for x < 60 mm, coinciding with low temperature regions where the jet impacts. NO levels along the centerline are seen to slightly increase with increasing distance from the injector. Overall, the main trends and levels are found to be well captured by the LES and to provide major improvements compared to previous studies [110]. The shape of the first profile, at x = 20 mm, is less well retrieved by the LES, with levels that are too high in the shear layer, consistent with levels found in the post-flame region and a flame front shifted towards smaller axial positions. Consistently with increasing temperature levels observed near the chamber's walls, Fig. 14(a), NO levels are found to increase past x > 60 mm. However, no data are available for these radial positions, preventing a deeper discussion.

5. Conclusion

This paper summarizes recent efforts towards the inclusion of a more comprehensive chemistry description in CFD applications. In particular, a multi-reduction automated tool, YARC, was employed to derive LES-compliant ARCs for various hydrocarbons and applications. The methodology is proven to be very efficient, enabling specifically to fully control stiffness and the maximum allowed error on targeted quantities. One major finding of this study is that any hydrocarbon, from the smallest -methane or ethylene, to the heavier multi-component aviation kerosenes can be directly accommodated in modern CFD applications, with the current available CPU resources. Combined with the Dynamically Thickened Flame (DTFLES) model, an ARC for a real aviation kerosene is used to simulate a Jet A fueled lab-scale burner. Comparisons with temperature and species data demonstrate the improved predictive capabilities of the present method, when compared to previous studies. Opportunities for further work are still largely open. The development of new reduction techniques and their more efficient implementation in multi-reduction tools are currently under investigation. These, coupled with a more rigorous stiffness estimation, would further extend the applicability of ARC in CFD. The derivation of ARC for bio-fuels will be investigated in the near future.

The reported ARCs are made available to the community, and can be found online [77].

Acknowledgments

The authors would like to thank Dr T. Jaravel, F. Collin-Bastiani, Dr. C. Lapeyre from the CFD team of CERFACS for providing their reduced mechanisms. Fruitful collaboration with the team of Prof. H. Wang is greatly appreciated. The authors also acknowledge the support from the Center for Turbulent Research (Stanford University-NASA AMES Research Center) as part of the work presented in this paper has been initiated during the 2016 Summer Program of this institute. Simulations were performed using HPC resources from GENCI-CCRT (Grant 2016-2b7525).

References

[1] A.H. Lefebvre, Gas Turbine Combustion, second ed., Taylor & Francis, 1998.
[2] D. Veynante, T. Poinsot, Reynolds averaged and Large-Eddy Simulation modeling for turbulent combustion, in: J. Ferziger, O. Metais (Eds.), New Tools in Turbulence Modelling. Lecture 5, Les editions de Physique, Springer, 1997, pp. 105–135.
[3] T. Baritaud, T. Poinsot, M. Baum, Direct Numerical Simulation for Turbulent Reacting Flows, Editions Technip, 1996.
[4] J.H. Chen, Petascale direct numerical simulation of turbulent combustion - fundamental insights towards predictive models, Proc. Combust. Inst. 33 (1) (2011) 99–123.
[5] T. Poinsot, D. Veynante, Theoretical and Numerical Combustion, second ed., R.T. Edwards, 2005 (out).
[6] C.K. Westbrook, Y. Mizobuchi, T.J. Poinsot, P.J. Smith, J. Warnatz, Computational combustion, Proc. Combust. Inst. 30 (1) (2005) 125–157.
[7] L.Y.M. Gicquel, G. Staffelbach, T.J. Poinsot, Large-Eddy Simulations of gaseous flames in gas turbine combustion chambers, Prog. Energy Combust. Sci. 38 (2012) 782–817.
[8] J. Warnatz, U. Maas, R.W. Dibble, Combustion: Physical and Chemical Fundamentals, Modeling and Simulation, Experiments, Pollutant Formation, (1995).
[9] T. Lu, C.K. Law, Toward accommodating realistic fuel chemistry in large-scale computations, Prog. Energy Combust. Sci. 35 (2) (2009) 192–215.
[10] B. Fiorina, D. Veynante, S. Candel, Modeling combustion chemistry in Large-Eddy Simulation of turbulent flames, Flow, Turbul. Combust. 94 (2015) 3–42.
[11] U. Maas, S.B. Pope, Simplifying chemical kinetics: intrinsic low-dimensional manifolds in composition space, Combust. Flame 88 (3) (1992) 239–264.
[12] O. Gicquel, N. Darabiha, D. Thévenin, Laminar premixed hydrogen/air counterflow flame simulations using flame prolongation of ildm with differential diffusion, Proc. Combust. Inst. 28 (2000) 1901–1908.
[13] J.A. Van Oijen, F.A. Lammers, L.P.H. De Goey, Modeling of complex premixed burner systems by using flamelet-generated manifolds, Combust. Flame 127 (3)

(2001) 2124–2134.
[14] C.D. Pierce, P. Moin, Progress-variable approach for Large-Eddy Simulation of non-premixed turbulent combustion, J. Fluid Mech. 504 (2004) 73–97.
[15] M. Philip, M. Boileau, R. Vicquelin, E. Riber, T. Schmitt, B. Cuenot, D. Durox, S. Candel, Large-Eddy Simulations of the ignition sequence of an annular multiple-injector combustor, Proc. Combust. Inst. 35 (3) (2015) 3159–3166.
[16] A. Avdić, G. Kuenne, F. di Mare, J. Janicka, LES combustion modeling using the eulerian stochastic field method coupled with tabulated chemistry, Combust. Flame 175 (2017) 201–219.
[17] L. Esclapez, P.C. Ma, E. Mayhew, X. Rui, S. Stouffer, T. Lee, H. Wang, M. Ihme, Fuel effects on lean blow-out in a realistic gas turbine combustor, Combust. Flame 181 (2017) 82–99.
[18] B. Fiorina, O. Gicquel, L. Vervisch, S. Carpentier, N. Darabiha, Approximating the chemical structure of partially premixed and diffusion counterflow flames using FPI flamelet tabulation, Combust. Flame 140 (3) (2005) 147–160.
[19] A.W. Vreman, B.A. Albrecht, J.A. Van Oijen, L. p. H. De Goey, R.J.M. Bastiaans, Premixed and non-premixed generated manifolds in large-eddy simulation of sandia flame D and F, Combust. Flame 153 (3) (2008) 394–416.
[20] E. Knudsen, H. Pitsch, A general flamelet transformation useful for distinguishing between premixed and non-premixed modes of combustion, Combust. Flame 156 (3) (2009) 678–696.
[21] P.-D. Nguyen, L. Vervisch, V. Subramanian, P. Domingo, Multidimensional flamelet-generated manifolds for partially premixed combustion, Combust. Flame 157 (1) (2010) 43–61.
[22] B. Franzelli, B. Fiorina, N. Darabiha, A tabulated chemistry method for spray combustion, Proc. Combust. Inst. 34 (1) (2013) 1659–1666.
[23] B. Fiorina, O. Gicquel, S. Carpentier, N. Darabiha, Validation of the FPI chemistry reduction method for diluted nonadiabatic premixed flames, Combust. Sci. Technol. 176 (5–6) (2004) 785–797.
[24] M. Ihme, H. Pitsch, Modeling of radiation and nitric oxide formation in turbulent nonpremixed flames using a flamelet/progress variable formulation, Phys. Fluids 20 (5) (2008) 055110.
[25] M.E. Mueller, H. Pitsch, LES model for sooting turbulent nonpremixed flames, Combust. Flame 159 (6) (2012) 2166–2180.
[26] C.K. Westbrook, F.L. Dryer, Simplified reaction mechanisms for the oxidation of hydrocarbon fuels in flames, Combust. Sci. Technol. 27 (1981) 31–43.
[27] W.P. Jones, R.P. Lindstedt, Global reaction schemes for hydrocarbon combustion, Combust. Flame 73 (3) (1988) 233–249.
[28] B. Franzelli, E. Riber, M. Sanjose, T. Poinsot, A two-step chemical scheme for kerosene–air premixed flames, Combust. Flame 157 (2010) 1364–1373.
[29] L. Selle, G. Lartigue, T. Poinsot, R. Koch, K.U. Schildmacher, W. Krebs, B. Prade, P. Kaufmann, D. Veynante, Compressible Large-Eddy Simulation of turbulent combustion in complex geometry on unstructured meshes, Combust. Flame 137 (2004) 489–505.
[30] C. Fureby, A comparative study of flamelet and finite rate chemistry LES for a swirl stabilized flame, J. Eng. Gas Turbines Power 134 (4) (2012) 041503.
[31] W.P. Jones, A. Tyliszczack, Large-eddy simulation of spark ignition in a gas turbine combustor, Flow, Turbul. Combust. 85 (3–4) (2010) 711–734.
[32] G. Lecocq, D. Poitou, I. Hernández, F. Duchaine, E. Riber, B. Cuenot, A methodology for soot prediction including thermal radiation in complex industrial burners, Flow, Turbul. Combust. 92 (2014) 947–970.
[33] T. Jaravel, Prediction of Pollutants in Gas Turbines Using Large-Eddy Simulation, Phd thesis CERFACS, 2016.
[34] N. Peters, B. Rogg, Reduced Kinetic Mechanisms for Applications in Combustion Systems. Lecture Notes in Physics vol. 15, Berlin Springer Verlag, 1993.
[35] J.F. Griffiths, Reduced kinetic models and their application to practical combustion systems, Prog. Energy Combust. Sci. 21 (1995) 25–107.
[36] S.T. Alison, T. Turányi, M.J. Pilling, Mathematical tools for the construction, investigation and reduction of combustion mechanisms. (Chap. 4), Compr. Chem. Kinet. 35 (1997) 293–437.
[37] D.A. Goussis, U. Mass, Model reduction for combustion chemistry, in: T. Echekki, E. Mastorakos (Eds.), Turbulent Combustion Modeling, Fluid Mechanics and its Applications, vol. 95, 2011, pp. 193–220.
[38] T. Turányi, Reduction of large reaction mechanisms, New J. Chem. 14 (1990) 795–803.
[39] T. Turányi, Sensitivity analysis of complex kinetic systems: tools and applications, J. Math. Chem. 5 (1990) 203–248.
[40] D.M. Hamby, A review of techniques for parameter sensitivity analysis of environmental models, Environ. Monit. Assess. 32 (1994) 135–154.
[41] S. Vadja, P. Valkó, T. Turányi, Principal component analysis of kinetic models, Int. J. Chem. Kinet. 17 (1985) 55–81.
[42] J. Revel, J.C. Boettner, M. Cathonnet, J.S. Bachman, Derivation of a global chemical kinetic mechanism for methane ignition and combustion, Journal de Chimie Physique 91 (4) (1994) 365–382.
[43] C.E. Frouzakis, K. Boulouchos, Analysis and reduction of the CH4-Air mechanism at lean conditions, Combust. Sci. Technol. 159 (2000) 281–303.
[44] T. Lu, C.K. Law, A directed relation graph method for mechanism reduction, Proc. Combust. Inst. 30 (2005) 1333–1341.
[45] T. Lu, M. Plomer, Z. Luo, S.M. Sarathy, W.J. Pitz, S. Som, D.E. Longman, Directed relation graph with expert knowledge for skeletal mechanism reduction, 7th US National Combustion Meeting, 2011.
[46] R. Sankaran, E.R. Hawkes, J.H. Chen, T.F. Lu, C.K. Law, Structure of a spatially developing turbulent lean methane–air bunsen flame, Proc. Combust. Inst. 31 (1) (2007) 1291–1298.
[47] P. Pepiot-Desjardins, H. Pitsch, An efficient error propagation based reduction method for large chemical kinetic mechanisms, Combust. Flame 154 (2008) 67–81.
[48] H. Huang, M. Fairweather, J.F. Griffiths, A.S. Tomlin, R.B. Brad, A systematic lumping approach for the reduction of comprehensive kinetic models, Proc. Combust. Inst. 30 (2005) 1309–1316.
[49] P. Pepiot, H. Pitsch, A chemical lumping method for the reduction of large chemical kinetic mechanisms, Combust. Theor. Model. 12 (6) (2008) 1089–1108.
[50] D.A. Goussis, S.H. Lam, A study of homogeneous methanol oxidation kinetics using CSP, Symp. (Int.) Combust. 24 (1) (1992) 113–120.
[51] H.S. Lam, D.A. Goussis, The CSP method for simplifying kinetics, Int. J. Chem. Kinet. 26 (1994) 461–486.
[52] T. Lovas, D. Nilsson, F. Mauss, Automatic reduction procedure for chemical mechanisms applied to premixed methane/air flames, Proc. Combust. Inst. 28 (2000) 1809–1815.
[53] P. Pepiot, Automatic Strategies to Model Transportation Fuel Surrogates, Phd thesis Stanford University, 2008.
[54] A.C. Zambon, H.K. Chelliah, Explicit reduced reaction models for ignition, flame propagation, and extinction of C2H4/CH4/H2 and air systems, Combust. Flame 150 (1) (2007) 71–91.
[55] T. Turányi, J. Tóth, Comments to an article of Frank-Kamenetskii on the quasi-steady-state approximation, Acta Chim. Hung. 129 (1992) 903–903.
[56] M.D. Smooke, V. Giovangigli, Reduced Kinetic Mechanisms and Asymptotic Approximations for Methane–Air Flames. Lecture Notes in Physics vol. 15, Springer-Verlag, 1991.
[57] T. Turányi, List of publications including reduced mechanisms for combustion applications, http://garfield.chem.elte.hu/Turanyi/ttpub.html, (1981).
[58] S. Liu, J.C. Hewson, J.H. Chen, H. Pitsch, Effects of strain rate on high-pressure nonpremixed n-heptane autoignition in counterflow, Combust. Flame 137 (3) (2004) 320–339.
[59] X. You, F.N. Egolfopoulos, H. Wang, Detailed and simplified kinetic models of n-dodecane oxidation: the role of fuel cracking in aliphatic hydrocarbon combustion, Proc. Combust. Inst. 32 (1) (2009) 403–410.
[60] A. Felden, Development of Analytically Reduced Chemistries (ARC) and Applications in Large Eddy Simulations (LES) of Turbulent Combustion, Phd thesis CERFACS, 2017.
[61] S. Navarro-Martinez, A. Kronenburg, LES/CMC simulations of a turbulent bluff-body flame, Proc. Combust. Inst. 31 (2) (2007) 1721–1728.
[62] W.P. Jones, A.J. Marquis, V.N. Prasad, LES of a turbulent premixed swirl burner using the eulerian stochastic field method, Combust. Flame 159 (10) (2012) 3079–3095.
[63] A. Giusti, E. Mastorakos, Detailed chemistry LES/CMC simulation of a swirling ethanol spray flame approaching blow-off, Proc. Combust. Inst. 36 (2) (2017) 2625–2632.
[64] S. Gallot-Lavallee, W.P. Jones, Large-Eddy Simulation of spray auto-ignition under EGR conditions, Flow, Turbul. Combust. 96 (2016) 513–534.
[65] T. Jaravel, E. Riber, B. Cuenot, G. Bulat, Large-Eddy Simulation of an industrial gas turbine combustor using reduced chemistry with accurate pollutant prediction, Proceedings of the Combustion Institute, 2016.
[66] O. Schulz, T. Jaravel, T. Poinsot, B. Cuenot, N. Noiray, A criterion to distinguish autoignition and propagation applied to a lifted methane–air jet flame, Proc. Combust. Inst. 36 (2) (2017) 1637–1644.
[67] A. Felden, E. Riber, B. Cuenot, Impact of direct integration of Analytically Reduced Chemistry in LES of a sooting swirled non-premixed combustor, Combust. Flame 191 (2018) 270–286.
[68] B. Franzelli, A. Vié, M. Boileau, B. Fiorina, N. Darabiha, Large-Eddy Simulation of swirled spray flame using detailed and tabulated chemical descriptions, Flow, Turbul. Combust. (2016) 1–29.
[69] A. Felden, L. Esclapez, E. Riber, B. Cuenot, H. Wang, Including real fuel chemistry in LES of turbulent spray combustion, Combust. Flame 193 (2018) 397–416.
[70] P. Dagaut, M. Cathonnet, The ignition, oxidation, and combustion of kerosene: a review of experimental and kinetic modeling, Prog. Energy Combust. Sci. 32 (1) (2006) 48–92.
[71] R. Xu, H. Wang, D.F. Davidson, R.K. Hanson, C.T. Bowman, F.N. Egolfopoulos, Evidence supporting a simplified approach to modeling high-temperature combustion chemistry, 10th US National Meeting on Combustion, College Park, MD, 2017.
[72] Y. Gao, T. Lu, R. Xu, H. Wang, D.F. Davidson, C.T. Bowman, R.K. Hanson, A Reduced Chemistry Model for Jet Fuel Combustion, (2015) Personal communication.
[73] T. Lu, C.K. Law, A criterion based on computational singular perturbation for the identification of quasi steady state species: a reduced mechanism for methane oxidation with no chemistry, Combust. Flame 154 (4) (2008) 761–774.
[74] T. Lu, C.K. Law, Strategies for mechanism reduction for large hydrocarbons: n-heptane, Combust. Flame 154 (1) (2008) 153–163.
[75] A.S. Tomlin, M.J. Pilling, T. Turányi, Mechanism reduction for the oscillatory oxidation of hydrogen: sensitivity and quasi-steady-state analyses, Combust. Flame 91 (1992) lO7–130.
[76] T. Lu, Reduced Mechanisms for Combustion Applications, (2008) http://www.engr.uconn.edu/tlu/mechs/mechs.htm.
[77] CERFACS, YARC Derived ARCs for Combustion Applications, (2017) http://www.cerfacs.fr/cantera.
[78] T. Turányi, L. Zalotai, S. Dobe, T. Berces, Applications of sensitivity analysis to combustion chemistry, Reliab. Eng. Syst. Saf. 57 (1997) 41–48.
[79] J.Y. Chen, Development of reduced mechanisms for numerical modelling of turbulent combustion, Workshop on Numerical Aspects of Reduction in Chemical Kinetics, CERMICS-ENPC, Cite Descartes, Champus sur Marne, France, Reno, NV, 1997.

[80] R.J. Kee, F.M. Rupley, J.A. Miller, Chemkin-II: A Fortran Chemical Kinetics Package for the Analysis of Gas-phase Chemical Kinetics. Technical Report SAND-89-8009, Sandia National Labs., Livermore, CA (USA), 1989.
[81] A. Massias, D. Diamantis, E. Mastorakos, D.A. Goussis, An algorithm for the construction of global reduced mechanisms with CSP data, Combust. Flame 117 (1999) 685–708.
[82] B. Rogg, A Computer Program for the Simulation of One-Dimensional Chemically Reacting Flows. Technical Report CUED/A-THERMO/TR39, Cambridge University, 1991.
[83] N. Jaouen, An Automated Approach to Derive and Optimise Reduced Chemical Mechanisms for Turbulent Combustion, Phd thesis CORIA, 2017.
[84] H. Pitsch, FlameMaster v3.1. A C++ Computer Program for 0D Combustion and 1D Laminar Fame Calculations, (1988).
[85] C.T. Bowman, R.K. Hanson, D.F. Davidson, W.C. Gardiner Jr., V. Lissianski, G.P. Smith, D.M. Golden, M. Frenklach, M. Goldenberg, GRI-mech 2.11, (1995) http://www.me.berkeley.edu/gri-mech.
[86] C.T. Bowman, M. Frenklach, W.R. Gardiner, G. Smith, The GRI-Mech 3.0 Chemical Kinetic Mechanism, University of California, Berkeley, CA, 1999.
[87] S. Mouriaux, Large Eddy Simulation of the Turbulent Spark Ignition and of the Flame Propagation in Spark Ignition Engines, Phd thesis EM2C, 2016.
[88] K. Narayanaswamy, G. Blanquart, H. Pitsch, A consistent chemical mechanism for oxidation of substituted aromatic species, Combust. Flame 157 (2010) 1879–1898.
[89] S. Jerzembeck, N. Peters, P. Pepiot-Desjardins, H. Pitsch, Laminar burning velocities at high pressure for primary reference fuels and gasoline: experimental and numerical investigation, Combust. Flame 156 (2) (2009) 292–301.
[90] Lawrence Livermore National Laboratory, Primary Reference Fuels (PRF): Iso-Octane/N-Heptane Mixtures, (2004) https://combustion.llnl.gov/archived-mechanisms/surrogates/prf-isooctane-n-heptane-mixture.
[91] B. Rochette, F. Collin-Bastiani, L. Gicquel, O. Vermorel, D. Veynante, T. Poinsot, Influence of chemical schemes, numerical method and dynamic turbulent combustion modeling on LES of premixed turbulent flames, Combust. Flame 191 (2018) 417–430.
[92] B. Sirjean, E. Dames, D.A. Sheen, H. Wang, A Simplified Version of the High-Temperature Chemical Kinetic Model of N-Alkane Oxidation, JetSurF Version 1.0, (2009) https://web.stanford.edu/group/haiwanglab/JetSurF/JetSurF1.0/Reduced Model/JetSurF1.0-l.html.
[93] B. Sirjean, E. Dames, D.A. Sheen, X.-Q. You, C. Sung, A.T. Holle, F.N. Egolfopoulos, H. Wang, S.S. Vasu, D.F. Davidson, R.K. Hanson, H. Pitsch, C.T. Bowman, A. Kelley, C.K. Law, W. Tsang, N.P. Cernansky, D.L. Miller, A. Violi, R.P. Lindstedt, A High-Temperature Chemical Kinetic Model of N-Alkane Oxidation, JetSurF Version 1.0, (2009) http://web.stanford.edu/group/haiwanglab/JetSurF/JetSurF1.0/index.html.
[94] H. Wang, X. You, A.V. Joshi, S.G. Davis, A. Laskin, F. Egolfopoulos, C.K. Law, USC Mech Version II. High-Temperature Combustion Reaction Model of H2/CO/C1-C4 Compounds, (2007) http://ignis.usc.edu/USC_Mech_II.htm.
[95] M. Bauerheim, T. Jaravel, L. Esclapez, E. Riber, L.Y.M. Gicquel, B. Cuenot, M. Cazalens, S. Bourgois, M. Rullaud, Multiphase flow Large-Eddy Simulation study of the fuel split effects on combustion instabilities in an ultra-low-nox annular combustor, J. Eng. Gas Turbines Power 138 (6) (2016) 061503.
[96] T. Edwards, L.Q. Maurice, Surrogate mixtures to represent complex aviation and rocket fuels, J. Propuls. Power 12 (2) (2001).
[97] H. Wang, R. Xu, K. Wang, C.T. Bowman, R.K. Hanson, D.F. Davidson, K. Brezinsky, F.N. Egolfopoulos, A physics-based approach to modeling real-fuel combustion chemistry-I. Evidence from experiments, and thermodynamic, chemical kinetic and statistical considerations, Combust. Flame 193 (2018) 502–519.
[98] R. Xu, K. Wang, S. Banerjee, et al., A physics-based approach to modeling real-fuel combustion chemistry–II. Reaction kinetic models of jet and rocket fuels, Combust. Flame 193 (2018) 520–537.
[99] J. Luche, Obtention de modeles cinétiques réduits de combustion. Application à un mécanisme du kérosène, Phd thesis Université d'Orléans, 2003.
[100] R. Xu, D. Chen, K. Wang, Y. Tao, J.K. Shao, T. Parise, Y. Zhu, S. Wang, R. Zhao, D.J. Lee, F.N. Egolfopoulos, D.F. Davidson, R.K. Hanson, C.T. Bowman, H. Wang, Hychem model: application to petroleum-derived jet fuels, 10th US National Meeting on Combustion, College Park, MD, 2017.
[101] A. Felden, E. Riber, B. Cuenot, L. Esclapez, M. Ihme, H. Wang, Including real fuel chemistry in LES of turbulent combustion, Proc. Of the Summer Program, Center for Turbulence Research, Stanford Univ., 2016, pp. 113–122.
[102] J. Cai, S.-M. Jeng, R. Tacina, The structure of a swirl-stabilized reacting spray issued from an axial swirler, 43 Rd AIAA Aerospace Sciences Meeting and Exhibit, 2005.
[103] Y. Fu, S.-M. Jeng, R. Tacina, Characteristics of the swirling flow generated by an axial swirler, ASME Turbo Expo 2005: Power for Land, Sea, and Air, American Society of Mechanical Engineers, 2005, pp. 517–526.
[104] A. Iannetti, N.-S. Liu, F. Davoudzadeh, The Effect of Spray Initial Conditions on Heat Release and Emissions in LDI CFD Calculations, NASA Glenn Research Center, Cleveland, OH, 2008 NASA Report No. NASA/TM—2008-214522.
[105] O. Colin, M. Rudgyard, Development of high-order taylor-galerkin schemes for LES, J. Comput. Phys. 162 (2000) 338–371.
[106] F. Nicoud, H. Baya Toda, O. Cabrit, S. Bose, J. Lee, Using singular values to build a subgrid-scale model for Large-Eddy Simulations, Phys. Fluids 23 (8) (2011) 085106.
[107] O. Colin, F. Ducros, D. Veynante, T. Poinsot, A thickened flame model for Large-Eddy Simulations of turbulent premixed combustion, Phys. Fluids 12 (7) (2000) 1843–1863.
[108] F. Charlette, D. Veynante, C. Meneveau, A power-law wrinkling model for LES of premixed turbulent combustion: Part I - non-dynamic formulation and initial tests, Combust. Flame 131 (2002) 159–180.
[109] B. Abramzon, W. Sirignano, Droplet vaporization model for spray combustion calculations, Int. J. Heat Mass Transf. 32 (9) (1989) 1605–1618.
[110] H. El-Asrag, A. Iannetti, S. Apte, Large eddy simulations for radiation-spray coupling for a lean direct injector combustor, Combust. Flame 161 (2) (2014) 510–524.